Available online at https://jcst.rsu.ac.th
Formerly Rangsit Journal of Arts and Sciences (RJAS)

Journal of Current Science and Technology, January-June 2020 JCST Vol. 10 No. 1, pp. 1-19

ISSN 2630-583 (Print)/ISSN 2630-656 (Online)

A novel approach and analysis for PV firming using grid-tied three-port microinverter

Mahmood Alharbi[1*] and Issa Batarseh[2]

[1]Department of Electrical Engineering, Taibah University, Medina 42353, Saudi Arabia
E-mail: maotay1988@gmail.com
[2]Department of Electrical and Computer Engineering, University of Central Florida, Orlando, FL 32816, United States
E-mail: issa.batarseh@gmail.com

*Corresponding Author

Received 28 February 2020, Revised 29 March 2020; Accepted 30 March 2020
Published online 31 March 2020

Abstract

With the demand increase for electricity, the ever-increasing awareness of environmental issues, coupled with rolling blackouts, the role of renewable energy generation will become even more significant. In this paper, a novel strategy is proposed that can harvest stable solar power despite of intermittency in solar irradiance, where a panel-level three-port grid-tied PV microinverter system is used instead of the traditional high-power energy storage and management system at the utility scale to implement PV firming. The microinverter system is composed of a front-end flyback converter and an H-bridge for inverter/rectifier, with battery stack connected to the DC-link. The proposed PV firming strategy lies in static and dynamic algorithms to generate smooth PV reference power, and the outcomes are implemented then to various control methods to charge/discharge the battery stack so that a stable power generation profile is obtained. Further, topology, simulation and experimental results are presente. Real-time PV intermittency and usable capacity data were discussed and analyzed in MATLAB/SIMULINK to validate the PV firming control. The experimental results verify the proposed PV firming algorithms.

Keywords**:** *dynamic algorithm, DC/DC converter, DC/AC inverter, energy storage, PV firming, three-port microinverter*

1. Introduction

In recent decades, several researches have paid more attention considerably on the renewable energy worldwide, where electricity generation by photovoltaic (PV) is becoming one of the most common clean and abundance renewable energy source. Although PV is highly nature dependent device and has ever decreasing cost, it has several technical challenges which effect on its penetration limit into the grid. Solar PV power generation has highly natural instability due to the irregular changes in the sun irradiance level effected by weather changing and cloud passing unless it is clear sky. Cloud passing effects on the PV have been studied for a long time (Jewell & Ramakumar, 1987; Kern & Gulachenski, 1989; Woyte, Thong, Belmans, & Nijs, 2006; Garrett & Jeter, 1989; Zabalawi, Mandic, & Nasiri, 2008). Some studies address this problem as a contemporaneous issue (Trueblood et al., 2013; Alam, Muttaqi, & Sutanto, 2014a), and focus on the high penetration level of PV generation.

Several undesirable effects of the PV variability are voltage fluctuations at the distribution system level, and frequency instability in small grids. The voltage fluctuations can lead to voltage flicker and excessive Load Tap Changer (LTC) operation. In small grids, the frequency instability can lead to increased damage to conventional voltage regulator equipment. These effects provide more challenges to higher penetration of PV in general and at the distribution levels particularly.

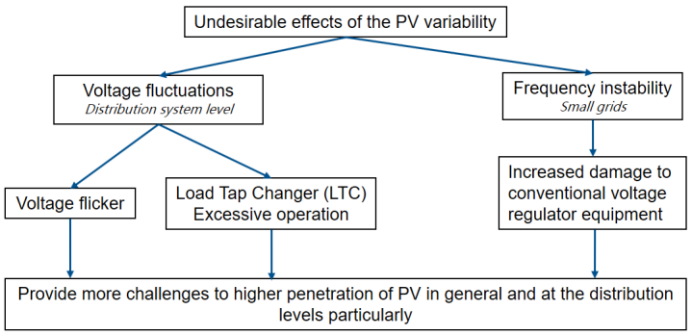

Figure 1 Summary for undesirable effects of the PV variability

Figure 1 summarizes these effects in flowchart. Generally, these renewables energies are unreliable and often applied concurrently with electrical energy storage systems to enhance their reliability in the network (Bird et al., 2013). This enhancement is by reducing the power fluctuations, improving the power quality, and enhancing the system flexibility. So, distributed energy storage seems to hold the key in unlocking the full potential of the renewable energy resources. Recent studies have focused on battery storage at both utility and distributed scale. Many advantages (e.g. energy arbitrage, increased PV self-consumption, transmission congestion relief, VAR support etc.) of such storage across various players ranging from independent system operators to end users are extensively reported earlier by these research works (Alam, Muttaqi, & Sutanto, 2013; Bortolini, Gamberi, & Graziani, 2014; Han, Ji, Zhao, & Zhang, 2015; Zhang, Lundblad, Campana, & Yan, 2016; Fthenakis, Mason, & Zweibel, 2009; Cucchiella, Adamo, & Gastaldi, 2016; Solomon, Faiman, & Meron, 2012).

Several types of technologies based on energy storage have been proposed for firming the PV output power. Different kinds of storages have been used, such as, battery energy storage (Hund, Gonzalez, & Barrett, 2010; Traube et al., 2013), fuel cell energy (Rahman & Tam, 1988), superconductive magnetic energy storage (Tam, Kumar, & Foreman, 1989), and electric double-layer capacitor (EDLC) (Kakimoto, Satoh, Takayama, & Nakamura, 2009; Kinjo, Senjyu, Urasaki, & Fujita, 2006; Monai, Takano, Nishikawa, & Sawada, 2004). In (Hund et al., 2010), a high-power level system of grid-tied PV firming has been implemented using a valve regulated lead-acid (VRLA) battery temporarily to charge and discharge as required for firming the inverter output power. A moving average calculation was used in (Hund et al., 2010; Kakimoto et al., 2009) to control the inverter output power by averaging the solar irradiance over the previous one-hour time interval. Another method to smooth the PV output power is by using battery energy storage system (BESS) as in (Li, Hui, & Lai, 2013), in which a large-scale BESS system was communicated with PV and wind power systems through the grid. The firming control used was based on the storage capacity, where the charging/ discharging scenarios were according to the state of charge (SOC) of the batteries. PV fluctuation ramp-rate can be assumed as rapid changings with different values of slope. Those changes can be compensated to maintain minimum value of slope as in (Alam, Muttaqi, & Sutanto, 2014b). Although the control strategy was independent on the previous PV intermittency history, it still makes delayed results practically. In (Abdelrazek and Kamalasadan, 2016a and Abdelrazek and Kamalasadan, 2016b), the algorithm of firming was based on maximum and minimum power reference for the PV output. Two bidirectional conversion systems were connected to the BESS for charging and discharging through the grid. A high-pass filter was used for fluctuation mitigation in (Traube et al., 2013). Such the corner frequency, as one of the filter characteristics, was being used to limit the ramp-rate of the PV inverter. In (Tesfahunegn, Ulleberg, Vie, & Undeland, 2011), the method that has been used for PV-firming is the exponential moving average.

JCST Vol. 10 No. 1 Jan.-Jun. 2020, pp. 1-19
ISSN 2630-0583 (Print)/ISSN 2630-0656 (Online)

Most of the reviewed technologies for the PV-firming are applied for high power level (PV arrays and energy storage stations). However, modular level systems (PV panel with micro-inverter and integrated storage) will be a future focus for solar PV deployment because of several remarkable merits. The speed response of the PV-firming method defers if the method is calculation-based or comparison-based. In the proposed algorithms, the PV output power is compared to a specified reference and then the output firmed profile is deployed. This results in high speed response that takes micro-seconds. In contrast, other methods depend on mathematical calculations such as applying traditional/exponential moving average method.

In this paper, a novel approach is developed where batteries are integrated directly on the DC-link of a PV-microinverter (H-bridge) with a flyback converter forming the first power conversion stage, resulting three-port microinverter (Alharbi, Pise, Haibing, & Batarseh, 2017; Alharbi, Pise, Haibing, & Batarseh, 2018). The major focus of this paper lies in the PV firming algorithms and the control strategy to charge/discharge the batteries so that a firmed power profile can be generated through the inverter stage. With these development targets, the research objectives of this paper are to design and implement a smart integration of the battery into the grid-tied power electronics without additional conversion stage, to design and implement a control method that is used for battery charging and discharging, and to design and implement new algorithms that are used for firming the PV output profile. In Section 2, the topology used and implemented controls without firming algorithm are discussed. The PV firming algorithms and analysis, consisting of static PV reference generation method, analysis of usable storage capacity when static reference used, dynamic PV reference generation algorithm, and battery charging/discharging algorithm are proposed in Section 3. In Section 4, MATLAB/SIMULINK simulations are performed, and the relevant waveforms are shown. Experimental validation of the proposed schemes is shown in Section 5.

2. The topology used and operational principle

2.1 The topology

The proposed grid-tied three-port bidirectional microinverter is given in Figure 2. This microinverter can interface battery, PV panel, and the grid. This two-stage converter is directly obtained from well-known flyback converter and H-bridge inverter topologies. In order to disconnect the battery, a relay switch is required. The active components and the relay are controlled to interface with the three different ports and regulate their power flows, voltages, and currents.

The flyback (DC-DC) stage is used to step up the PV voltage to produce a nominal DC-link voltage of 225V. The H-bridge (DC-AC) stage is used for inverting the DC-link voltage to the AC voltage (grid) of 120V RMS. The third port of battery is connected in parallel to the DC-link. Because of the battery flexibility in voltage with respect to its size, it is designed to make the battery voltage the same as the DC-link voltage without having to use an additional stage for battery power conversion. The proposed topology has the capability to operate in six different scenarios, PV to Grid, PV to Grid/Battery (charging), PV/Battery to Grid (discharging), PV/Grid to Battery (charging), Battery to Grid (discharging), and Grid to Battery (charging).

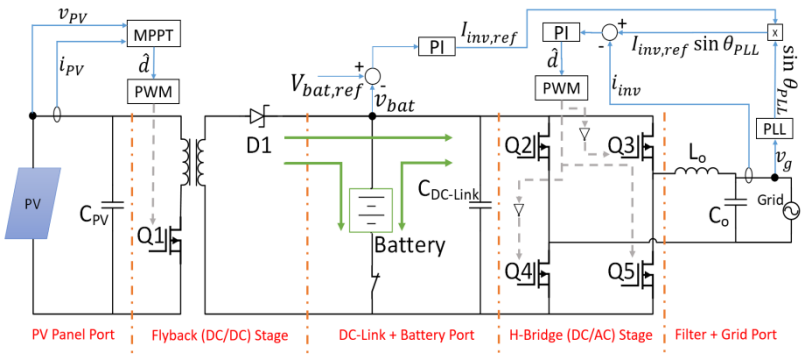

Figure 2 The proposed grid-tie three-port PV microinverter

2.2 Implemented controls regardless of the proposed algorithms

A full overview of the system controls implemented regardless of the PV-firming algorithms is represented in Figure 2. Starting with the PV source, a maximum power point tracking (MPPT) algorithm is used to control the flyback DC/DC converter. It does this according to the maximum power delivered from the PV. In this topology, the author has used the Perturbation and Observation (P&O) technique. The objective of the P&O algorithm is to track the PV voltage and current to maintain the maximum power. Then, the duty value for the flyback is set according the reference PV voltage chosen by the algorithm when the power is maximized. A phase-locked loop (PLL) controller is required when the grid is one of the ports in this system. Basically, the PLL functions to track the phase and frequency of the fundamental grid voltage. This results in a pure sine wave, which matches the grid's characteristics with a unit amplitude. The two conversion stages in the proposed systems are interfaced through a DC-link. They must be maintained with a regulated voltage. Therefore, a DC-link voltage regulation control (DCVR) must be implemented. The purpose of the DCVR is to balance the power into and out of the DC-link. In addition, a reference current amplitude is generated for the inverter stage ($I_{inv,ref}$). This reference value is multiplied by the sine wave generated by the PLL. This produces a reference current for the inverter output current regulation (OCR) control loop. After multiplying the reference amplitude of the inverter output current ($I_{inv,ref}$) by the unity sinusoidal function ($\sin(\theta_{PLL})$) generated by the PLL, the OCR will be operated.

3. The proposed PV firming algorithms and analysis

In order to interface with a third source of power such as battery, an additional control algorithm must be implemented. In this research, the proposed algorithm that controls the battery power for either being charged or discharged depends on a reference of an output power profile. Static PV reference generation method with storage capacity sizing analysis, dynamic PV reference generation algorithm with storage capacity sizing analysis, and the battery charging/discharging algorithm are discussed in this section.

3.1 Static PV firming approach

3.1.1 Static PV reference generation method

The static PV reference generation method is based on a historical data of PV intermittency for a specific region or area. East Florida is the region selected by the author in this research, where the data has been collected online by Florida Solar Energy Center at University of Central Florida, Cocoa campus ("PV Intermittency Data," n.d.). Data was collected from a combination of two 300W PV modular systems consisting of PV panel and grid-tied microinverter.

The East Florida region static PV reference power ($P_{PV,ref}$) is calculated by averaging daily data for each month with resolution of a minute ("PV Intermittency Data," n.d.). Each month is assumed to have specific average PV reference power ($P_{ref,avg}$), which is calculated using equations (1) and (2).

$$P_{ref,avg}(t) = \left\{P_{ref,avg}^{m_1}, P_{ref,avg}^{m_2}, \dots, P_{ref,avg}^{m_k}\right\} \quad (1)$$

$$P_{ref,avg}^{m_n} = \frac{\sum_{d_1}^{d_l}\left(P_{ref,avg}^{m_n}(d_n)\right)}{l} \quad (2)$$

where, $m_1, m_2, m_3 \dots m_k$ correspond to the minutes over a day. k: is equal to 1440, which is the total minutes in each day. $d_1, d_2, d_3 \dots d_l$: correspond to the days over each month. l: is the last day of each month. $P_{PV,avg}^{m_n}$: is the nth minute's average value of PV power in a month.

A similar method is applied for the calculating the maximum PV reference power ($P_{ref,max}$) using equations (3) and (4). This maximum reference will be used and discussed later for performing the dynamic method. Figure 3 shows examples of energy reference power profiles for two different days selected randomly in 2016 (Feb. 19th and Aug. 17th). Each month has different maximum and average PV reference power curves, because they are in different seasons. Noticeably, the actual PV power (orange solid) curve of each example is fluctuating up/ down around the average PV reference power (red dashed) curve and under the maximum PV reference power (blue solid) curve.

$$P_{ref,max}(t) = \left\{P_{ref,max}^{m_1}, P_{ref,max}^{m_2}, \dots, P_{ref,max}^{m_k}\right\} \quad (3)$$

$$P_{ref,max}^{m_n} = Max_{d_1}^{d_l}\left\{P_{ref,max}^{m_n}(d_n)\right\} \quad (4)$$

where, $P_{ref,max}^{m_n}$ is the n[th] minute's maximum value of PV power in a month.

3.1.2 Storage capacity sizing analysis for the static PV reference

Energy data was collected for two PV modular systems with 600W total power in ("PV Intermittency Data," n.d.), where each system consists of a PV panel and grid-tied microinverter. A monthly average PV reference power is generated and passed through another algorithm of charging/discharging control where the static PV firming algorithm is assumed to be applied. Based on this assumption, the PV energy is calculated and analyzed for each month to conclude with an average usable storage capacity.

Since this analysis objective is to calculate the average usable battery capacity for each month, average PV energy ($\boldsymbol{E}_{PV,avg}$), maximum PV energy ($\boldsymbol{E}_{PV,max}$), and minimum PV energy ($\boldsymbol{E}_{PV,min}$) are calculated, as follows.

Equation (5) defines the total average PV energy which is calculated by integrating the average energy for every minute ($E_{PV,avg}^{m_n}$) given in (6). $E_{PV,avg}^{m_n}$ is calculated by averaging the energy at that moment over one complete month.

$$\boldsymbol{E}_{PV,avg} = \int E_{PV,avg}(t)dt \quad (5)$$

$$E_{PV,avg}(t) = \left\{E_{avg}^{m_1}, E_{avg}^{m_2}, \dots, E_{avg}^{m_k}\right\} \quad (6)$$

$$E_{PV,avg}^{m_n} = \frac{\sum_{d_1}^{d_l}\left(E_{avg}^{m_n}(d_n)\right)}{l} \quad (7)$$

where, $E_{PV,avg}^{m_n}$: is the PV energy at the n[th] minute averaged correspondingly over a month.

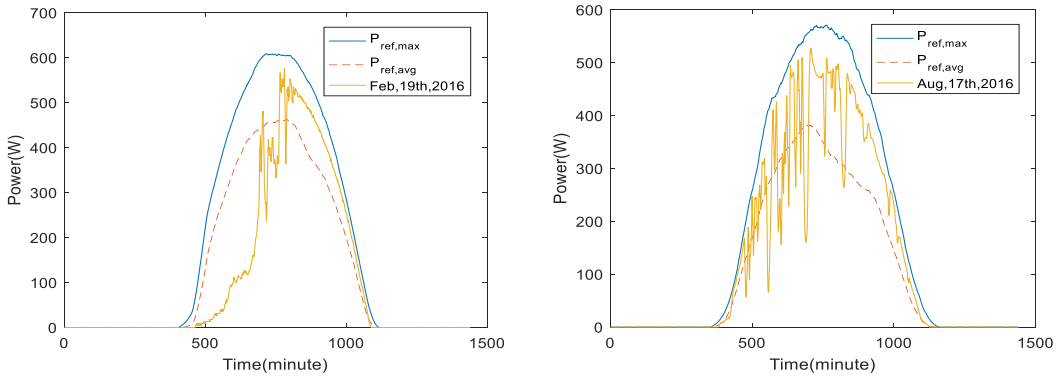

(a) (b)

Figure 3 Maximum and average PV reference power compared to PV actual power on two different days in 2016

Similar method is applied for the maximum PV energy ($\boldsymbol{E}_{PV,max}$) and the minimum PV energy ($\boldsymbol{E}_{PV,min}$), as follows.

$$\boldsymbol{E}_{PV,max} = \int E_{PV,max}(t)dt \quad (8)$$

$$E_{PV,max}(t) = \left\{E_{PV,max}^{m_1}, E_{PV,max}^{m_2}, \dots, E_{PV,max}^{m_k}\right\} \quad (9)$$

$$E_{PV,max}^{m_n} = Max_{d_1}^{d_l}\left\{E_{PV,max}^{m_n}(d_n)\right\} \quad (10)$$

$$\boldsymbol{E}_{PV,min} = \int E_{PV,min}(t)dt \quad (11)$$

$$E_{PV,min}(t) = \left\{E_{PV,min}^{m_1}, E_{PV,min}^{m_2}, \dots, E_{PV,min}^{m_k}\right\} \quad (12)$$

$$E_{PV,min}^{m_n} = Min_{d_1}^{d_l}\left\{E_{PV,min}^{m_n}(d_n)\right\} \quad (13)$$

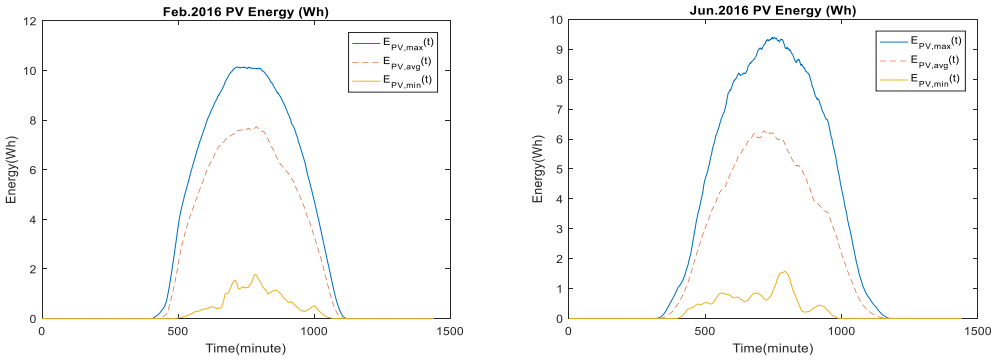

(a) (b)

Figure 4 Average, maximum, and minimum PV energy for month of (a) Feb. 2016 and (b) Jun. 2016

Two examples are plotted in Figure 4 for two different months, February and June, in 2016, where the total average PV energy is around 3.2kWh in February, and around 2.7kWh in June.

Now, the average usable storage capacity can be calculated where the PV output profile is assumed to be firmed on the average PV power statically. Also, it is assumed to have both maximum and minimum energy on same day. So, the average PV energy curve ($E_{PV,avg}(t)$) is considered as the PV firming reference power. The area between the maximum PV energy curve ($E_{PV,max}(t)$) and the $E_{PV,avg}(t)$ is considered as the average surplus PV energy to be stored in the storage ($E_{PV,surplus}$). However, the area between the $E_{PV,avg}(t)$ and the minimum PV energy curve ($E_{PV,min}(t)$) is considered as the average insufficient PV energy ($E_{PV,insufficient}$). The difference between $E_{PV,surplus}$ and $E_{PV,insufficient}$ is defined as the average usable storage (battery) capacity ($E_{bat,cap}$) needed to maintain the static PV firming output profile, which is given in (14).

$$E_{bat,cap} = \left|E_{PV,surplus} - E_{PV,insufficient}\right| \quad (14)$$

where,

$$E_{PV,surplus} = \int E_{PV,max}(t)dt - \int E_{PV,avg}(t)dt = E_{PV,max} - E_{PV,avg} \quad (15)$$

$$E_{PV,insufficient} = \int E_{PV,avg}(t)dt - \int E_{PV,min}(t)dt = E_{PV,avg} - E_{PV,min} \quad (16)$$

Figure 5 represents a summary for the analyzed average usable storage capacity that is assumed to be needed according to the data collected for each month.

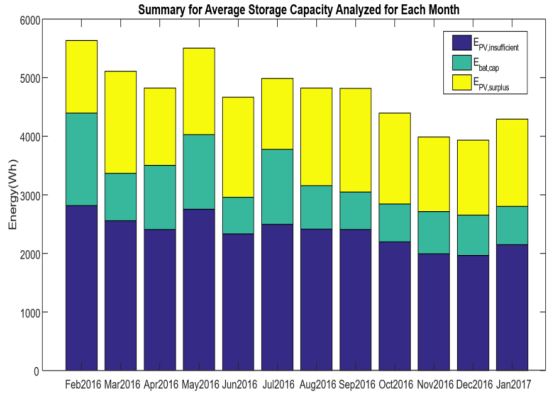

Figure 5 Analysis of PV and average storage capacities when the system is assumed to be firmed statically

As a result of this analysis, the average usable storage capacity ranges between around 628Wh (Jun. 2016) and 1.6kWh (Feb. 2016). Thus, if the static algorithm is assumed to be implemented in reality, the average usable capacity of storage that would be integrated to 600W system is around 1.6kWh, hence the average nominal storage capacity would be up to 3.2kWh. However, if the worst case is assumed when having only minimum PV energy, the actual usable storage capacity would be much larger than average, which might be up to 3kWh (up to 6kWh nominal capacity of battery). This is an obvious drawback of the static algorithm. Therefore, a dynamic PV firming algorithm is encouraged to be proposed.

3.2 Dynamic PV firming approach

3.2.1 Dynamic PV reference generation algorithm

In this proposed dynamic PV reference generation algorithms, one static reference must be computed and coded, and by which several layers will be generated accordingly. By comparing the actual PV power to the layers, the PV reference power will be generated dynamically.

The dynamic reference generation algorithm depends on three main factors. The first factor is the maximum PV reference curve ($P_{ref,max}$) formulated in (3) and (4), by which several layers are generated. It can be assumed as a map for the final generated reference power, and it changes monthly based on the analysis of collected data at Central Florida (example) location ("PV Intermittency Data," n.d.). Second, the fluctuation factor (*ls*) which controls the smoothness of the generated reference curve and determines the number of comparable layers (No. of layers = 1/*ls*) as shown in Figure 6 Since the layer curves are generated by the $P_{ref,max}$, the only saved data in the memory is $P_{ref,max}$. And third, the slew power ($P_{PV,act}$) from abrupt changes as well as the smoothness. It is defined as a factor of a slope equation as in (17) or (18).

$$\sigma_f P_{ref,max}(i) = \frac{d(i)}{\Delta t} \tag{17}$$

$$\sigma_f P_{ref,max}(i) = \frac{df(i)}{\Delta t} \tag{18}$$

where, $d(i)$ is the PV actual power change difference as given in (19). $df(i)$ is the difference between the current $P_{PV,act}$ and the previous $P_{PV,ref}$ as given in (20).Δt is the time difference and is assumed to be 1 minute since data changes every minute.

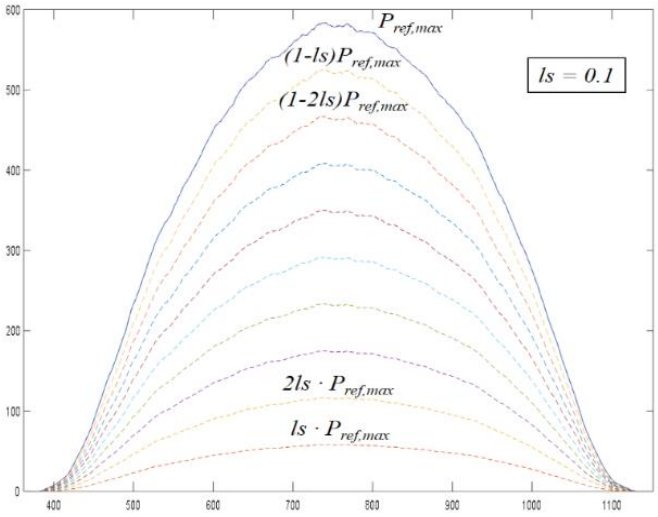

Figure 6 The maximum PV reference power with generated layers

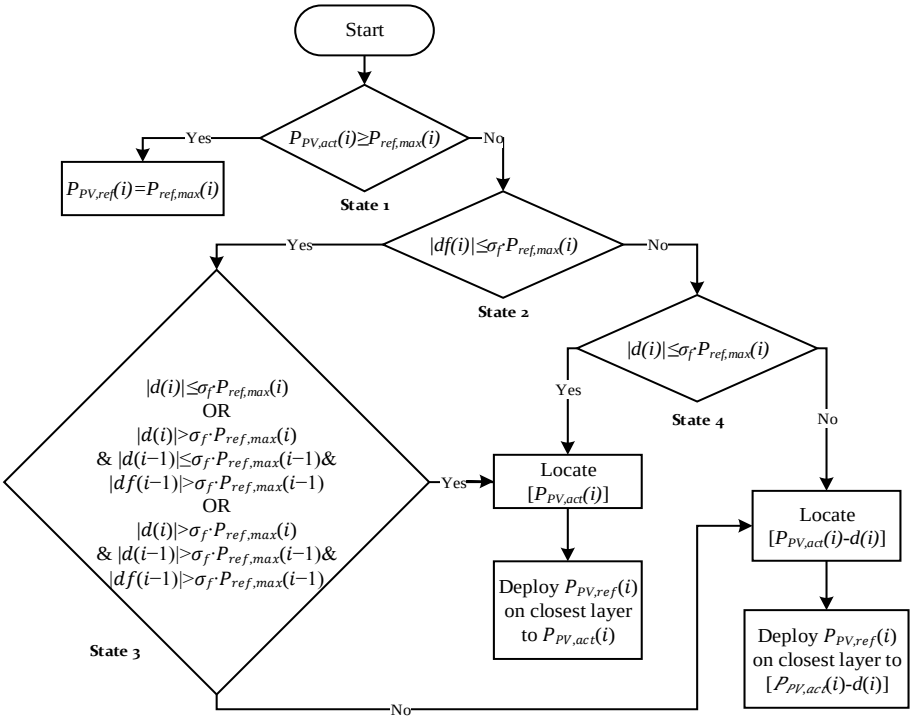

Figure 7 Proposed algorithm for dynamic PV reference power generation

Figure 7 illustrates the flowchart of the dynamic $P_{PV,ref}$ generation algorithm. The algorithm begins by comparing the current value of the $P_{PV,act}(i)$ with $P_{ref,max}$, designated as state 1. If $P_{PV,act}(i)$ is greater than or equal to $P_{ref,max}$, the generated $P_{PV,ref}$ will be maintained to $P_{ref,max}$. State 2, state 3, and state 4 depend on two variables; the PV actual power change difference ($d(i)$) in (19) and the difference between the current $P_{PV,act}$ and the previous $P_{PV,ref}$, which is $df(i)$ in (20). First variable of $d(i)$ determines the ramp rate of the current PV actual power ($P_{PV,act}(i)$) compared to the previous PV actual power value ($P_{PV,act}(i-1)$), which means actual power change per minute. It is named actual-actual ramp rate. Second variable of $df(i)$ determines the ramp rate of the $P_{PV,act}(i)$ compared to the previous PV generated reference power ($P_{PV,ref}(i-1)$). It is named actual-reference ramp rate. If $P_{PV,act}(i)$ is below $P_{ref,max}$, state 2 evaluates the fluctuation by comparing the absolute value of $df(i)$ to the maximum fluctuating value in the current time ($\sigma_f \cdot P_{ref,max}$). This process determines how the current PV power is ramped up/down compared to the previous PV firmed value, which means that how the actual-reference ramp rate is changing currently. If $|df(i)|$ is less than or equal to ($\sigma_f \cdot P_{ref,max}$) which means that it has low ramp rate, state 3 assures that the $P_{PV,act}$ is not fluctuating, by comparing $d(i)$ and $df(i)$ to ($\sigma_f \cdot P_{ref,max}(i)$). State 3 is used to ascertain that the $P_{PV,act}(i)$ is consistent. If state 2 is false, another comparison between *d(i)* and ($\sigma_f \cdot P_{ref,max}(i)$) is calculated to assure that the $P_{PV,act}(i)$ is not fluctuating as in state 4. If either state 3 or state 4 is true, the location of the $P_{PV,act}(i)$ is defined. Then, the generated $P_{PV,ref}$ is deployed on the closest layer to the current value of $P_{PV,act}$. If either state 3 or state 4 is false, which implies that the $P_{PV,act}$ has abrupt change (high slew rate), the location of the $[P_{PV,act}(i) - d(i)]$ is defined. Then, the generated $P_{PV,ref}$ is deployed on the closest layer to the current value of $[P_{PV,act}(i) - d(i)]$.

$$d(i) = P_{PV,act}(i) - P_{PV,act}(i-1) \quad (19)$$

$$df(i) = P_{PV,act}(i) - P_{PV,ref}(i-1) \quad (20)$$

Two examples of dynamic PV firming reference generation are shown in Figure 8. They

are intermittencies for two different days. In Figure 8 (a), the slew rate factor (σ_f) is equal to 0.03 which means that the generated PV reference power ($P_{PV,ref}$) ramps by 3% of the maximum PV reference power ($P_{ref,max}$) curve or less. The fluctuation factor (*ls*) is equal to 0.25 implying that there are 4 comparable layers, where the output is as smooth as each layer. In Figure 8 (b), the $P_{PV,ref}$ ramps by 7% of the $P_{ref,max}$ curve or less. The PV actual power ($P_{PV,act}$) is being compared to 5 different layers.

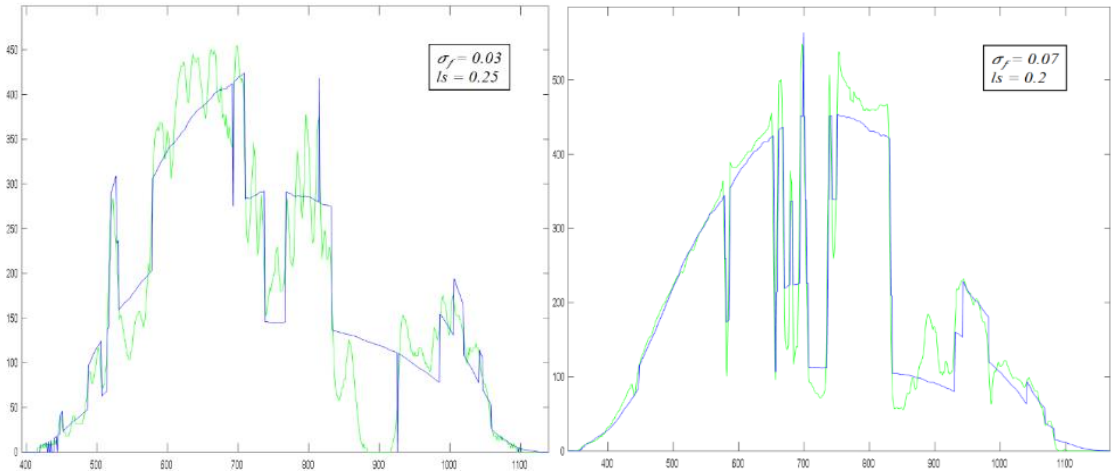

(a) (b)

Figure 8 Generated PV firming reference for two different days

In the next step, the generated PV reference profile is used in another algorithm of PV firming battery charge/discharge control to produce the final power profile through the three-port microinverter.

3.2.2 Storage capacity sizing analysis for the dynamic PV reference

For the dynamic PV firming, the main factor that can determine the storage capacity sizing is the fluctuation factor (*ls*). Therefore, in addition to controlling the smoothness of the output power profile, there are other relationships between the number of power levels or the fluctuation factor (*ls*) and the usable storage capacity ($E_{bat,cap}$), the surplus PV energy to be stored in the storage ($E_{PV,surplus}$), and the deficient PV energy ($E_{PV,deficient}$). An example for analysis and discussion is presented in Figure 9.

Initially, the slew rate factor (σ_f) must be fixed while the *ls* is being changed. Then, for every adjustment of *ls*, the $E_{bat,cap}$, the $E_{PV,surplus}$, and the $E_{PV,deficient}$ need to be calculated. There are two different methods for calculating these energies.

The first method is to determine the difference between the PV actual power ($P_{PV,act}$) and the generated PV reference power ($P_{PV,ref}$) for every minute that $P_{PV,act}$ is greater/ less than $P_{PV,ref}$. The results are calculated in total to determine the energy. When $P_{PV,act}$ is greater than $P_{PV,ref}$, the $E_{PV,surplus}$ is resulted. Otherwise, it results the $E_{PV,deficient}$. The following equations represent the calculations for this method.

$$E_{PV,surplus} = \left[\sum_t P_{PV,act}(t)\,\delta t - \sum_t P_{PV,ref}(t)\,\delta t\right], \quad P_{PV,act} > P_{PV,ref} \tag{21}$$

$$E_{PV,deficient} = \left[\sum_t P_{PV,ref}(t)\,\delta t - \sum_t P_{PV,act}(t)\,\delta t\right], \quad P_{PV,ref} > P_{PV,act} \tag{22}$$

The $E_{bat,cap}$ is determined in (14).

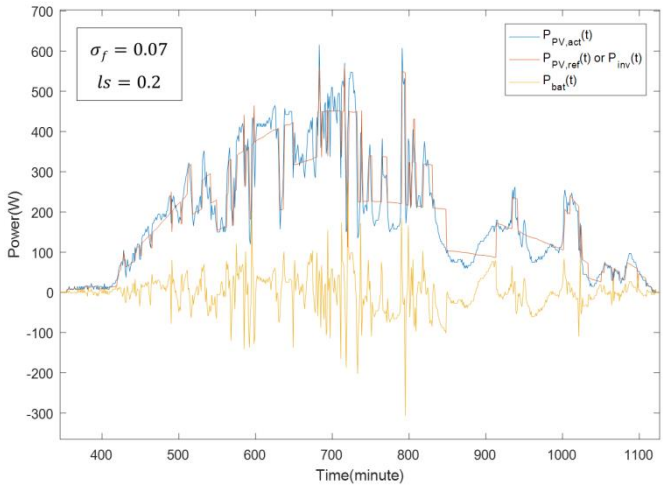

Figure 9 Power waveforms of PV actual (blue), PV reference/firmed inverter output (red), and battery (orange), such an example for a day in May 2016.

The other method is to calculate the total positive and negative values for the battery power (P_{bat}), where P_{bat} is the difference between $P_{PV,act}$ and $P_{PV,ref}$.

$$E_{PV,surplus} = \sum_t P_{bat}(t)\,\delta t, \quad P_{bat} > 0 \tag{23}$$

$$E_{PV,deficient} = -\sum_t P_{bat}(t)\,\delta t, P_{bat} < 0 \tag{24}$$

As shown in Figure 10, the fluctuation factor (*ls*) or the number of power levels (1/ *ls*) has an obvious effect on the energy capacity of the storage. The relationship of the surplus PV energy ($E_{PV,surplus}$) and the deficient PV energy ($E_{PV,deficient}$) to the *ls* seems linear until the *ls* is equal to about 0.15, or there are about 7 comparable power levels. Thus, the usable storage capacity ($E_{bat,cap}$) would have similar proportionality. Once the number of power levels decreases, or the *ls* increases after that point, the $E_{PV,surplus}$ starts decreasing gradually with respect to the *ls* while the $E_{PV,deficient}$ continues increasing linearly. Therefore, the $E_{bat,cap}$ will be enlarged since the PV energy is becoming much less sufficient. However, although decreasing the fluctuation factor (*ls*) (increasing the number of power levels) minimizes the storage capacity, it affects the smoothness negatively. As a result of this analysis, the storage capacity size can range from below 50Wh to above 200Wh (100Wh to 400Wh - nominal capacity value).

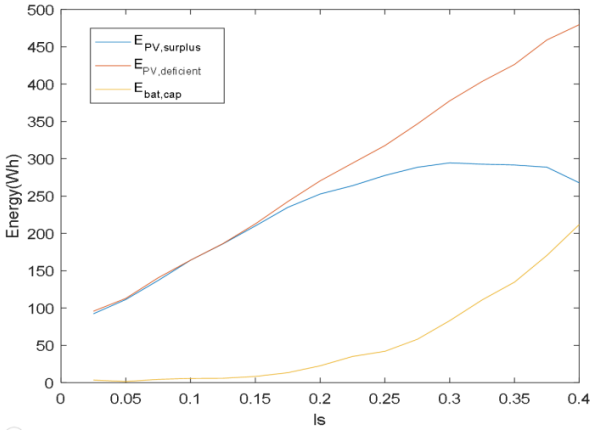

Figure 10 Analysis of PV and usable storage capacities when the system is firmed dynamically

JCST Vol. 10 No. 1 Jan.-Jun. 2020, pp. 1-19
ISSN 2630-0583 (Print)/ISSN 2630-0656 (Online)

Figures 11-12 illustrate the power waveforms for the example shown in Figure 9. Here, the fluctuation rate is decreased by increasing the fluctuation factor (*ls*). So, the conclusion is that the *ls* makes a trade-off between the fluctuation rates and the storage capacity sizing.

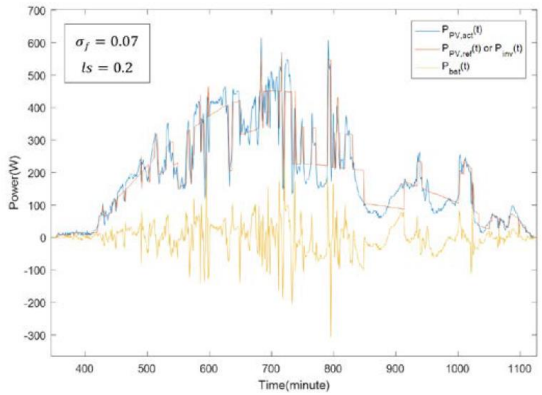

Figure 11 Power waveforms for same example shown in Figure 9 but with different fluctuation factor (*ls*=0.1)

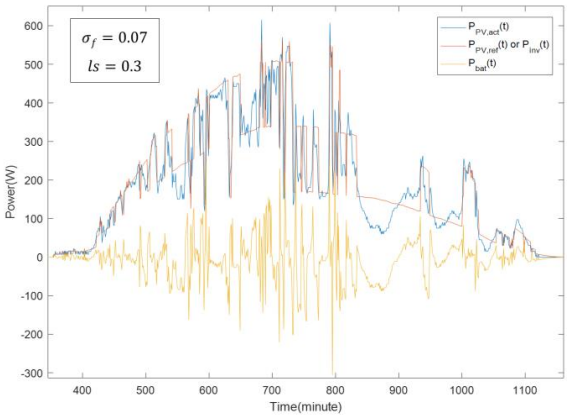

Figure 12 Power waveforms for same example shown in Figure 9 but with different fluctuation factor (*ls*=0.3)

3.3 Battery charging/discharging algorithm

Once the desired profile of the PV reference curve is generated, it is fed into the power electronics design through the microcontroller. It does this in order to control the battery charging discharging scenarios. An algorithm for charging/ discharging decisions is proposed in this research. Figure 13 illustrates the proposed architecture of the PV firming system with this algorithm added to the other controls mentioned in Section 2.

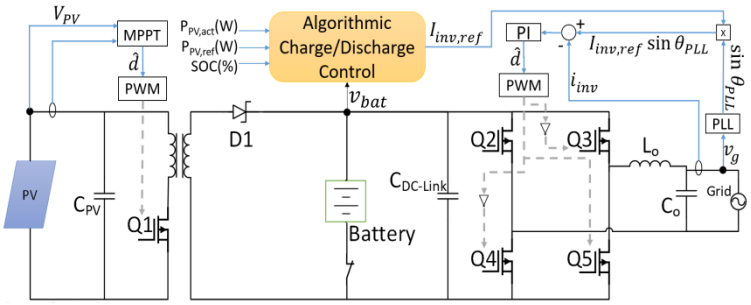

Figure 13 Architecture of the proposed PV firming system

In the battery charge/discharge control algorithm for the PV-firming in Figure 14, each process of the proposed algorithm will end up with two decisions. First, the generated value of the inverter reference current amplitude ($I_{inv,ref}$) is decided. This controls the battery current value (I_{bat}) simultaneously. Second, the decision of either charging, discharging, or disconnecting the battery occurs. Both decisions are based on four factors: the actual PV output power ($P_{PV,act}$), the generated PV reference power ($P_{PV,ref}$), the state of charge (SOC) of the battery energy, and the battery voltage (V_{bat}). The objective of the algorithm in Figure 14 is to make the $P_{PV,act}$ matched with the $P_{PV,ref}$ by charging/discharging the battery.

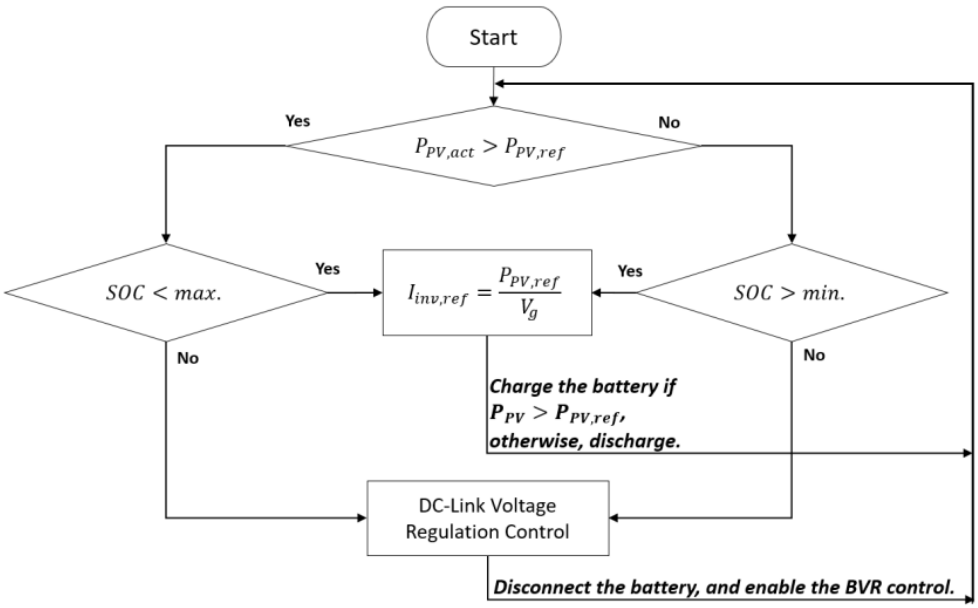

Figure 14 The algorithm flowchart for the PV firming battery charge/discharge control

The algorithm begins by comparing the generated PV reference power ($P_{PV,ref}$) to the actual PV power ($P_{PV,act}$) in real time. After each comparison, the state of charge (SOC) will be determined. When the $P_{PV,act}$ is greater than the $P_{PV,ref}$ and the SOC is less than its maximum percentage of energy, the battery is charged. The inverter reference current ($I_{inv,ref}$) is then calculated using equation (25). Whenever the $P_{PV,}$ is less than or equal to the $P_{PV,ref}$ and the SOC is greater than its minimum percentage of energy, the battery will be discharged. The $I_{inv,ref}$ is then again determined using equation (25). Equations (26) and (27) represent the ideal case of the battery current (I_{bat}) when it is being charged and discharged, respectively. This value for I_{bat} is

determined simultaneously with the inverter current value (I_{inv}).

$$I_{inv,ref} = \frac{P_{PV,ref}}{V_g} \quad (25)$$

$$I_{bat} = -\frac{P_{bat}}{v_{bat}} = I_{PV} - I_{inv} \quad (26)$$

$$I_{bat} = \frac{P_{bat}}{v_{bat}} = I_{inv} - I_{PV} \quad (27)$$

Since the DC-link has a constant voltage from the battery, there will not be a need to regulate control of the DC-link voltage. However, once the SOC is equal to its minimum or maximum percentage of energy, the battery is disconnected and the $I_{inv,ref}$ is generated by the DC-link voltage regulation control (DCVR) which is addressed previously in the section 2. This situation of disconnecting the battery is considered as rarely occurrence compared to being charged or discharged because of the instability of the PV power levels. Therefore, a power relay can be a suitable device to be implemented for disconnecting the battery. So, there are two different scenarios that provide the $I_{inv,ref}$, namely, charging/discharging scenario and DCVR scenario as clarified in Figure 15, where the concept of the DCVR is to balance between the power into and out of the DC-link. Additionally, a reference current amplitude for the inverter stage ($I_{inv,ref}$) is aimed to be generated and multiplied by the sine wave resulted from the PLL in order to generate a reference current for the inverter output current regulation (OCR) control loop as shown in Figure 2 and Figure 13. The block diagram of the DCVR control is shown in Figure 16.

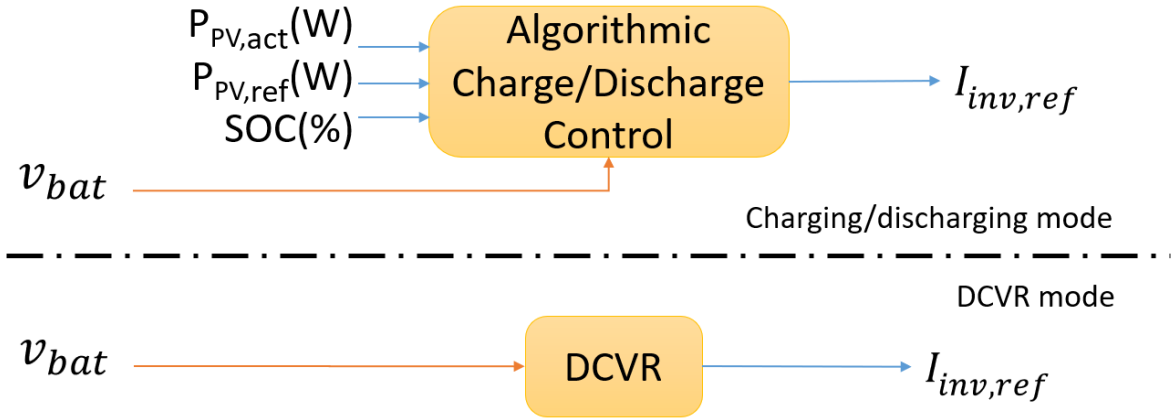

Figure 15 Scenarios configuration for the inverter reference current generation

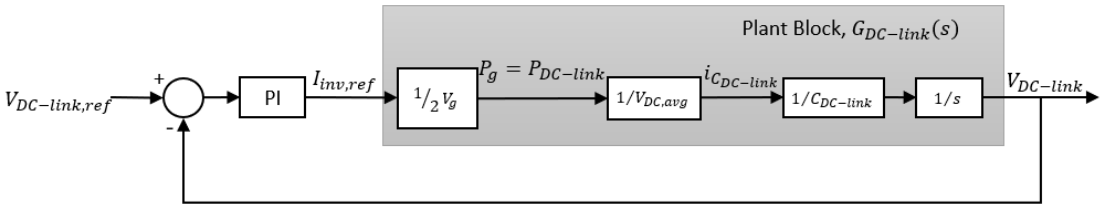

Figure 16 Block diagram for the DC-link voltage regulation (DCVR) control

When this $I_{inv,ref}$ is multiplied by half of the grid voltage amplitude, it results the grid average power. Using this information, the DC-link power ($P_{DC-link}$) is computed. Dividing the DC-link power by its average voltage ($V_{DC-link,0}$) produces its current ($i_{DC-link}$). Finally, the actual DC-link voltage is computed by dividing the integral of the DC-link current by its capacitor.

The plant transfer function (voltage-to-current) for DCVR is given in (28).

$$G_{DC-link}(s) = \frac{V_{DC-link}}{I_{inv,ref}} = \frac{V_g}{s2C_{DC-link}V_{DC-link,0}} \quad (28)$$

4. Simulation results

Simulations are carried out using MATLAB/Simulink to validate the proposed PV-firming algorithms on the grid-tied two-stage battery-integrated micro-system shown earlier in Figure 13. Power waveforms for the generated PV reference power ($P_{PV,ref}$), the PV actual power ($P_{PV,act}$), the inverter stage output power (P_{inv}), and the battery power (P_{bat}) for the static and dynamic PV firming microsystem are shown in Figure 17 and Figure 18, respectively. Since the MATLAB/Simulink simulations take a long time to perform the calculations, the timeline for the waveforms is scaled down to 24 seconds. This removes the rate fluctuations from consideration. The battery power (P_{bat}) is either positive indicating that the battery is discharging power to the grid, or negative indicating that the battery is being charged from the PV.

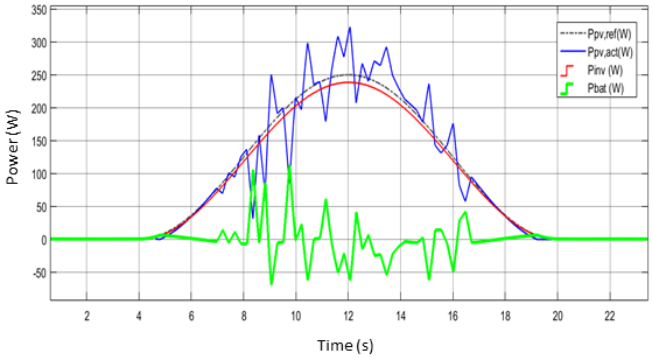

Figure 17 Power waveforms for PV reference (scatter black), PV actual (blue), firmed inverter output (red), and battery (green) for the static firming micro-system

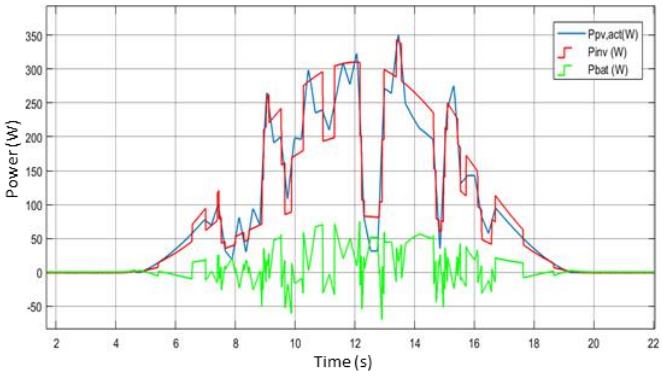

Figure 18 Power waveforms for PV reference (scatter black), PV actual (blue), firmed inverter output (red), and battery (green) for the dynamic firming micro-system

Table 1 Prototype specifications

Category	Value
Output Power	200W
PV Voltage	24~45V
Grid Voltage/ Frequency	~120V/ 60Hz
Battery Voltage	210~245V (Typically:225V)
Nominal Bus Voltage	225V

JCST Vol. 10 No. 1 Jan.-Jun. 2020, pp. 1-19
ISSN 2630-0583 (Print)/ISSN 2630-0656 (Online)

Table 2 Technical specifications of the battery used in the experiment

Specifications		Description
Voltage	Nominal	12V
	Cycle	14.5~14.9V
	Float	13.6~13.8V
Rated Capacity 77°F(25°C)		1.3Ah
Chemistry		Sealed Lead Acid (AGM - Absorbent Glass Mat)
Dimensions (mm/inch)	Length	97 (3.82)
	Wedth	43 (1.69)
	Height	52 (2.05)
	Total Height	58 (2.28)
Approx. Weight (kg/lbs)		0.6 (1.32)
Terminal		T1-A

5. Experimental results

To verify the proposed static PV-firming control algorithm experimentally, a 200W prototype is built with specifications as shown in Table 1. The prototype test set-up consists of Solar Array Simulator interfaced with AC Power Source/ Analyzer to represent the grid voltage and loaded with AC Electronic Load. The power waveforms are monitored by a Digital Power Analyzer, and the currents and voltages waveforms are monitored by a Digital Phosphor Oscilloscope. For experimental verification purpose, 18 counts of 12-volt lead acid battery (AJC-D1.3S) manufactured by AJC® Battery are connected in series. More specifications for the storage device that is used in the experimental set-up are shown in Table 2.

The experimental voltage and current waveforms for the PV output power ($P_{PV,act}$), inverter output power (firmed) (P_{inv}), and the battery power (P_{bat}) while charging and discharging for the static and dynamic PV firming system are shown in Figure 19 and Figure 20, respectively. The timeline for the waveforms is scaled down to around half an hour. So, the rates of fluctuations have been taken out of consideration. Since the $P_{PV,act}$ (blue curve) has been changed manually using the Solar Array Simulator, the PV output power curve does not display as much fluctuation as real-time power. However, the charging/discharging control algorithm is verified, since the P_{inv} (yellow) is following the generated PV reference power. The P_{bat} is either positive indicating that the battery is discharging power to the grid ($P_{PV,act}$ is greater than the generated PV reference), or negative indicating that the battery is being charged from the PV ($P_{PV,act}$ is less than the generated PV reference). Figure 21 shows experimental waveforms of the grid voltage (V_g), DC-link (battery) voltage ($V_{dc-link}$) along with inverter output current (I_{inv}) and battery current (I_{bat}) while the battery is being charged. Figure 22 shows the same waveforms while the battery is being discharged. Note that the positive battery current (I_{bat}) implies that the battery is being charged and similarly negative implies that battery is being discharged. The average value of $V_{dc-link}$ is about 236V in Figure 21 and 234V in Figure 22, which are in the specified range of the battery voltage. The V_g and I_{inv} are as pure sinusoidal as expected.

6. Conclusions

Algorithms and analysis for a PV firming system are proposed using a three-port microinverter topology in this paper. Batteries are seamlessly integrated with the flyback converter and H-bridge inverter as a third port in the microinverter. All implemented controls regardless of the PV firming algorithms are discussed. As a first step, a static PV reference power is generated by a proposed method. The usable energy storage has been analyzed for the system when it depends on static PV reference for firming, resulting that the nominal storage capacity reach up to 6kWh for 600W system. According to the analysis results for storage capacity sizing when the static algorithm is applied, the value of this novel dynamic PV reference generation algorithm for PV firming is supported. This results in an output power profile that can demonstrate minimal ramp-rate and reduced storage capacity.

In the final step of PV firming, the output of the static or dynamic PV reference generation algorithm becomes an input of the charging/discharging algorithm to control the battery power. The sizing of the storage capacity is analyzed for the system when it depends on dynamic PV reference for firming. This results in a nominal storage capacity changing form about 100Wh to 400Wh for 600W system. A PV firmed power profile is generated first in MATLAB/ SIMULINK with the proposed algorithms which are consequently validated experimentally. The experimental results have some errors compared to the simulation results. The error is based on the power rates. It ranges between about 4.5% (around 200W power rate) and 13.7% (around 12W power rate). The DC-link (battery) voltage and current, and the inverter output current and voltage are as expected. The overall system efficiency is not considered in this paper since the contributions are the algorithms and controls for the purpose of PV-firming which can be applicable to different topology and different power level.

To further improve the performance of the PV-firming algorithms, several research points should be considered. There are some high ramp-rate fluctuations which in some cases need to be filtered. Another research point is to find the optimal storage capacity based on the proposed PV-firming algorithm for this specific 200W panel-level system or even for different power level. For the battery charging/discharging algorithm, an additional factor would be considered in order to have a balanced case for charging/ discharging. In other words, the energy consumed while the battery is being discharged should be equivalent to that energy acquired while the battery is being charged.

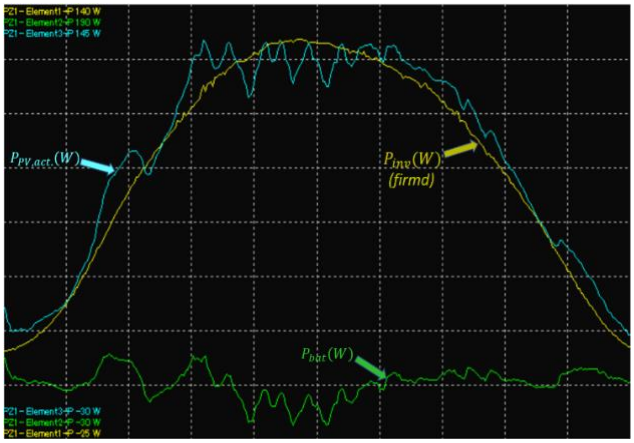

Figure 19 Power waveforms for PV actual, inverter output (firmed), and battery for static firming

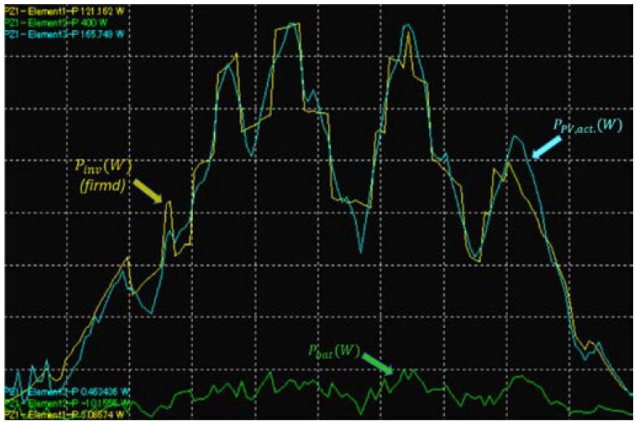

Figure 20 Power wave forms for PV actual, inverter output (firmed), and battery for dynamic firming

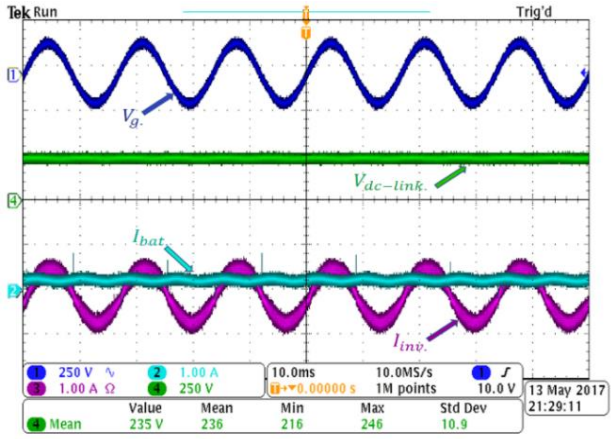

Figure 21 Voltages and currents waveforms while charging the battery

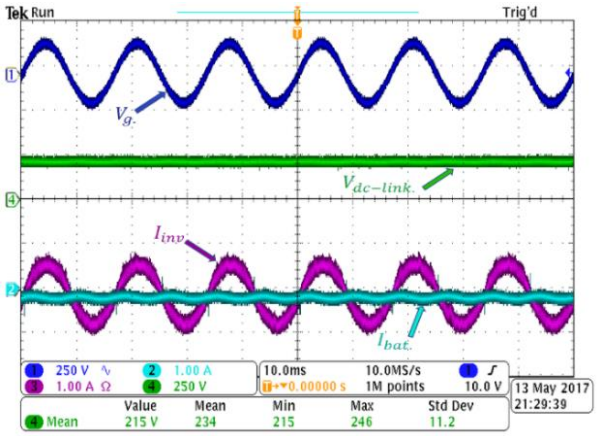

Figure 22 Voltages and currents waveforms while discharging the battery

7. References

Abdelrazek, S., & Kamalasadan, S. (2016a). A weather-based optimal storage management algorithm for PV capacity firming. *IEEE Transactions on Industry Applications*, *52*(6), 5175-5184. DOI: 10.1109/TIA.2016.2598139

Abdelrazek, S. A., & Kamalasadan, S. (2016b). Integrated PV capacity firming and energy time shift battery energy storage management using energy-oriented optimization. *IEEE Transactions on Industry Applications, 52*(3), 2607-2617. DOI: 10.1109/TIA.2016.2531639

Alam, M. J. E., Muttaqi, K. M., & Sutanto, D. (2013). Mitigation of rooftop solar PV impacts and evening peak support by managing available capacity of distributed energy storage systems. *IEEE Transaction on Power Systems*, *28*(4), 3874-3884. DOI: 10.1109/TPWRS.2013.2259269

Alam, M. J. E., Muttaqi, K. M., & Sutanto, D. (2014a). Mitigation of rapid voltage variations caused by passing clouds in distribution networks with solar PV using energy storage. In *8th International Conference on Electrical and Computer Engineering: Advancing Technology for a Better Tomorrow, ICECE 2014* (pp. 305-308). DOI:10.1109/ICECE.2014.7026821

Alam, M. J. E., Muttaqi, K.M., & Sutanto, D. (2014b). A novel approach for ramp-rate control of solar PV using energy storage to mitigate output fluctuations caused by cloud passing, IEEE Transactions on Energy Conversion, 29(2), 507-518. DOI: 10.1109/TEC.2014.2304951

Alharbi, M., Pise, A., Haibing, H., & Batarseh, I.

(2017). A new algorithm for PV firming using three-port micro-converter. In *2017 6th International Conference on Renewable Energy Research and Applications, ICRERA 2017* (pp. 719-722). San Diego, CA: IEEE. DOI; https://doi.org/10.1109/ICRERA.2017.8191154

Alharbi, M., Pise, A., Haibing, H., & Batarseh, I. (2018). A new dynamic PV firming control algorithm using grid-tied three-port micro-converter. In *2018 IEEE Applied Power Electronics Conference and Exposition (APEC)* (pp. 3200-3204). San Antonio, TX: IEEE. DOI: 10.1109/apec.2018.8341560

Bird, L., Milligan, M., Lew, D., Bird, L., Milligan, M., & Lew, D. (2013). Integrating variable renewable energy : Challenges and solutions integrating variable renewable energy : Challenges and solutions. *National Renewable Energy Laboratory (NREL)*. https://www.nrel.gov/docs/fy13osti/60451.pdf

Bortolini, M., Gamberi, M., & Graziani, A. (2014). Technical and economic design of photovoltaic and battery energy storage system. *Energy Conversion and Management*, *86*, 81-92. DOI: 10.1016/j.enconman.2014.04.089

Cucchiella, F., Adamo, I. D., & Gastaldi, M. (2016). Photovoltaic energy systems with battery storage for residential areas : An economic analysis international panel on climate change. *Journal of Cleaner Production*, *131*, 460-474. DOI:

Fthenakis, V., Mason, J. E., & Zweibel, K. (2009). The technical , geographical , and economic feasibility for solar energy to supply the energy needs of the US. *Energy Policy*, *37*, 387-399. DOI: 10.1016/j.enpol.2008.08.011

Garrett, D. L., & Jeter, S. M. (1989). A photovoltaic voltage regulation impact investigation technique: Part I - Model development. *IEEE Transactions on Energy Conversion*, *4*(1), 47-53. DOI: 10.1109/60.23149

Han, X., Ji, T., Zhao, Z., & Zhang, H. (2015). Economic evaluation of batteries planning in energy storage power stations for load shifting. *Renewable Energy*, *78*, 643-647. https://doi.org/10.1016/j.renene.2015.01.056

Hund, T. D., Gonzalez, S., & Barrett, K. (2010). Grid-tied PV system energy smoothing. In *2010 35th IEEE Photovoltaic Specialists Conference* (pp. 002762-002766). DOI: https://doi.org/10.1109/PVSC.2010.5616799

Jewell, W., & Ramakumar, R. (1987). The effects of moving clouds on electric utilities with dispersed photovoltaic generation. *IEEE Transactions on Energy Conversion*, *EC-2*(4), 570-576. DOI: 10.1109/TEC.1987.4765894

Kakimoto, N., Satoh, H., Takayama, S., & Nakamura, K. (2009). Ramp-rate control of photovoltaic generator with electric double-layer capacitor. *IEEE Transactions on Energy Conversion*, *24*(2), 465-473.

Kern, E. C., & Gulachenski, E. M. (1989). Cloud effects on distributed photovoltaic generation: slow transients at the Gardner, Massachusetts photovoltaic experiment. *IEEE Transactions on Energy Conversion*, *4*(2), 184-190. DOI: 10.1109/60.17910

Kinjo, T., Senjyu, T., Urasaki, N., & Fujita, H. (2006). Output levelling of renewable energy by electric double-layer capacitor applied for energy storage system. *IEEE Transactions on Energy Conversion*, *21*(1), 221-227. DOI: 10.1109/TEC.2005.853752

Li, X., Hui, D., & Lai, X. (2013). Battery energy storage station (BESS)-based smoothing control of photovoltaic (PV) and wind power generation fluctuations. *IEEE Transactions on Sustainable Energy*, *4*(2), 464-473. DOI: 10.1109/TSTE.2013.2247428

Monai, T., Takano, I., Nishikawa, H., & Sawada, Y. (2004). A collaborative operation method between new energy-type dispersed power supply and EDLC. *IEEE Transactions on Energy Conversion*, *19*(3), 590-598. DOI: 10.1109/TEC.2004.827714

Rahman, S., & Tam, K. S. S. (1988). A feasibility study of photovoltaic fuel cell hybrid

energy system. *IEEE Transactions on Energy Conversion*, *3*(1), 50-55. DOI: 10.1109/60.4199

Solomon, A. A., Faiman, D., & Meron, G. (2012). Appropriate storage for high-penetration grid-connected photovoltaic plants. *Energy Policy*, *40*(C), 335-344. DOI: 10.1016/j.enpol.2011.10.019

Tam, K.-S., Kumar, P., & Foreman, M. (1989). Enhancing the utilization of photovoltaic power generation by superconductive magnetic energy storage. *IEEE Transactions on Energy Conversion*, *4*(3), 314-321. DOI: 10.1109/60.43230

Tesfahunegn, S. G., Ulleberg, Ø., Vie, P. J. S., & Undeland, T. M. (2011). PV fluctuation balancing using hydrogen storage ― a smoothing method for integration of PV generation into the utility grid. *Energy Procedia*, *12*(1876), 1015-1022. DOI: https://doi.org/10.1016/j.egypro.2011.10.133

Traube, J., Lu, F., Maksimovic, D., Mossoba, J., Kromer, M., Faill, P., Casey, L. (2013). Mitigation of solar irradiance intermittency in photovoltaic power systems with integrated electric-vehicle charging functionality. *IEEE Transactions on Power Electronics*, *28*(6), 3058-3067. DOI: 10.1109/TPEL.2012.2217354

Trueblood, C., Coley, S., Key, T., Rogers, L., Ellis, A., Hansen, C., & Philpot, E. (2013). PV measures up for fleet duty: Data from a Tennessee plant are used to illustrate metrics that characterize plant performance. *IEEE Power and Energy Magazine*, *11*(2), 33-44. https://doi.org/10.1109/MPE.2012.2234405

Woyte, A., Thong, V. Van, Belmans, R., & Nijs, J. (2006). Voltage fluctuations on distribution level introduced by photovoltaic systems. *IEEE Transactions on Energy Conversion*, *21*(1), 202-209. DOI: 10.1109/TEC.2005.845454

Zabalawi, S. A., Mandic, G., & Nasiri, A. (2008). Utilizing energy storage with PV for residential and commercial use. In *34th Annual Conf. of IEEE Indust. Elect. (IECON), Orlando, FL* (pp. 1045-1050). https://doi.org/10.1109/IECON.2008.4758098

Zhang, Y., Lundblad, A., Campana, P. E., & Yan, J. (2016). Employing battery storage to increase photovoltaic self-sufficiency in a residential building of Sweden. *Energy Procedia*, *88*, 455-461. https://doi.org/10.1016/j.egypro.2016.06.025